Momentary High-Z Gate Driving (MHZGD) at Miller Plateau for IGBT Load Current Estimation from Gate Driver

Hiromu Yamasaki, Ryunosuke Katada, Katsuhiro Hata, and Makoto Takamiya

The University of Tokyo, Tokyo, Japan

***Abstract*—To eliminate a load current (I_L) sensor required to determine optimum gate driving parameters of a digital gate driver for IGBTs and to estimate I_L from the gate driver, a momentary high-Z gate driving (MHZGD) method is proposed. In MHZGD, the output voltage (V_{OUT}) of the gate driver is measured at Miller plateau when the gate driving current (I_G) is zero for a short time (1 µs in this paper), and I_L is estimated from the measured V_{OUT}. MHZGD is suitable for the digital gate driver, because the I_L estimation is not affected by I_G, and has the advantage of not affecting the switching operation of IGBT. In the double pulse test of IGBT at 300 V, by using one-point calibration at I_L = 20 A at 25 °C, the measured I_L estimation errors of three IGBTs in the range from 5 A to 80 A are within + 7.7 % / − 7.0 % at 25 °C, 75 °C, and 125 °C, which suggests that MHZGD can estimate I_L with acceptable error against IGBT and temperature variations.**

***Keywords*—digital gate driver, IGBT, load current, estimation**

I. Introduction

Active gate driving of IGBTs, where the gate driving current (I_G) is dynamically controlled during the turn-on/off transients, is a promising technology to solve the conventional trade-off between the switching loss and the current or voltage overshoot of IGBTs. Digital gate drivers (DGDs) [1] are useful for the active gate driving, because I_G is programmable with gate driving parameters using a software. In DGDs, however, gate driving parameters require information on load current (I_L) and junction temperature (T_J), because the optimum parameters depend on I_L and T_J [2]. Since adding a current sensor (e.g., current transformer, shunt resistor [3-4], and Rogowski coil [5-7]) to measure I_L is costly, I_L estimation method, which can be integrated on DGD IC, is preferable in terms of cost reduction.

Fig. 1 shows a circuit schematic of a gate driver and an IGBT. I_L can be estimated by Miller plateau voltage of the internal gate-emitter voltage ($V_{GE,INT}$) of IGBT, because the plateau voltage depends on I_L [8]. The target of this work is to estimate I_L from the output voltage (V_{OUT}) of the gate driver without depending on I_G. V_{OUT} and $V_{GE,INT}$, however, are not equal due to I_G ($R_{G,INT}$ + $R_{G,EXT}$) drop, where $R_{G,INT}$ and $R_{G,EXT}$ are the internal gate resistance of IGBT module and the external gate resistance, respectively. In [8], the relationship between I_L and the external gate-emitter voltage ($V_{GE,EXT}$) of IGBT module depends on I_G, which is not acceptable in DGDs, because I_G dynamically changes in DGDs. In [9], I_L is estimated from I_G, which cannot be used in the current-source based DGDs [1], because I_G is controlled by digital inputs and does not depend on I_L. To solve the problems, in this paper, a momentary high-Z gate driving (MHZGD) method is proposed to estimate I_L from V_{OUT} without depending on I_G.

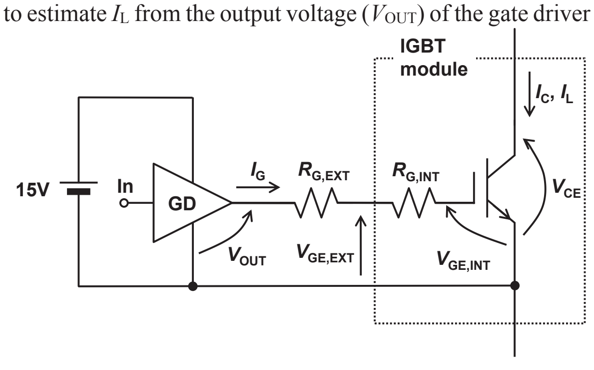

Fig. 1. Circuit schematic of gate driver and IGBT.

II. Proposed Momentary High-Z Gate Driving (MHZGD)

Figs. 2 and 3 show waveforms of a conventional gate driving and the proposed MHZGD at turn-on and turn-off of IGBT, respectively. In the conventional gate driving, V_{OUT} at the Miller plateau is not equal to $V_{GE,INT}$ due to I_G ($R_{G,INT}$ + $R_{G,EXT}$) drop. In MHZGD, however, I_G is zero during t_2 (1 µs in this paper) and the operation starts after turn-on or before turn-off. Zero I_G for a short time is the origin of name of MHZGD. In this work, the zero I_G is achieved using the current-source based DGD [1]. Even if the current-source based DGD is not available, any gate driver can implement MHZGD if a switch is added between the output of the gate driver and the gate of IGBT, and the switch is turned off for a short time. The period of t_2 must be after the switching of the collector current (I_C) and the collector-emitter voltage (V_{CE}) at turn-on (Fig. 2) and before the switching of I_C and V_{CE} at turn-off (Fig. 3) to avoid the increase of switching loss, and must be within the Miller plateau of $V_{GE,INT}$. During t_2, V_{OUT} is equal to $V_{GE,INT}$ because of zero I_G, and this V_{OUT} is defined as $V_{OUT,MHZ}$. Therefore, in MHZGD, I_L can be estimated from

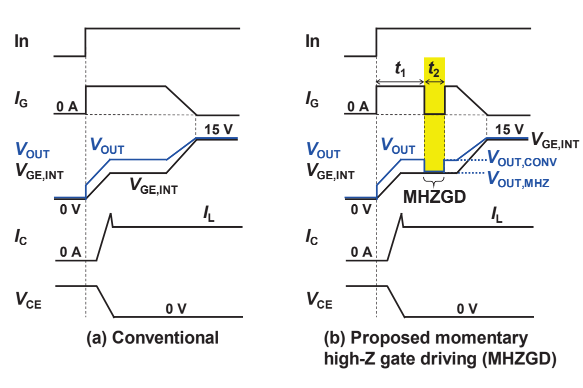

Fig. 2. Waveforms of conventional gate driving and proposed MHZGD at turn-on of IGBT.

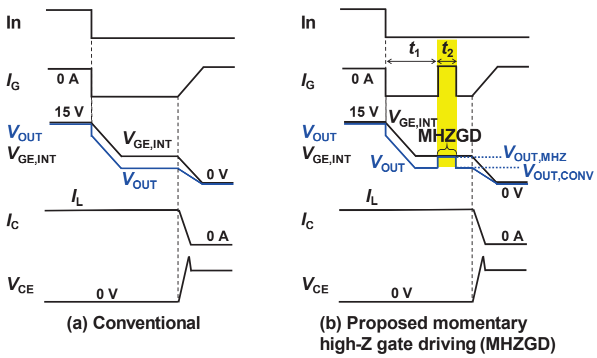

Fig. 3. Waveforms of conventional gate driving and proposed MHZGD at turn-on of IGBT.

$V_{OUT,MHZ}$ (= $V_{GE,INT}$). The measurement of $V_{OUT,MHZ}$ can be done with an A/D converter, which can be integrated on DGD IC. V_{OUT} just before the period of t_2 is defined as $V_{OUT,CONV}$.

Fig. 4 shows the photo of the measurement setup of the double pulse test of the IGBT module (2MBI100VA-060-50, 600 V, 100 A) at 300 V to demonstrate MHZGD. The current-source based DGD IC [1] drives the low side of the IGBT module. $R_{G,EXT}$ is zero. In this paper, I_L estimations at different IGBT modules, T_J's, and I_G's are discussed. Figs. 5 (a) and (b) show the measured waveforms at I_L = 50 A, T_J = 25 °C, and t_2 = 1 µs during the turn-on and turn-off of IGBT, respectively. $V_{OUT,MHZ}$ generated by MHZGD is clearly observed. Please note that MHZGD has no effect on the switching loss and overshoots of I_C and V_{CE}. Figs. 6 (a) and (b) show the measured V_{OUT} waveforms of I_L = 5 A, 50 A and 80 A at T_J = 25 °C during the turn-on and turn-off of IGBT, respectively. $V_{OUT,MHZ}$ increases with increasing I_L. Figs. 7 (a) and (b) show the measured V_{OUT} waveforms of two different I_G's at I_L = 50 A and T_J = 25 °C during the turn-on and turn-off of IGBT, respectively. Please note that $V_{OUT,MHZ}$'s of the two curves are the same independent of I_G. Figs. 8 (a) and (b) show the measured I_L dependence of $V_{OUT,CONV}$ and $V_{OUT,MHZ}$ of two different I_G's at T_J = 25 °C during the turn-on and turn-off of IGBT, respectively. $V_{OUT,CONV} - V_{OUT,MHZ}$ is 0.68 V at I_G = 78 mA during the turn-on and $V_{OUT,MHZ} - V_{OUT,CONV}$ is 0.68 V at I_G = 78 mA during the turn-off, which are reasonably explained by $I_G \times R_{G,INT}$ = 78 mA × 9 Ω = 0.70 V. Both $V_{OUT,CONV}$ and $V_{OUT,MHZ}$ depend on I_L. $V_{OUT,CONV}$ depends on I_G, while $V_{OUT,MHZ}$ does not depend on I_G, which clearly shows that proposed MHZGD estimates I_L independent of I_G. As expected, the curve of $V_{OUT,MHZ}$ in Fig. 8 (a) matches the curve of $V_{OUT,MHZ}$ in Fig. 8 (b) and the proposed MHZGD works for

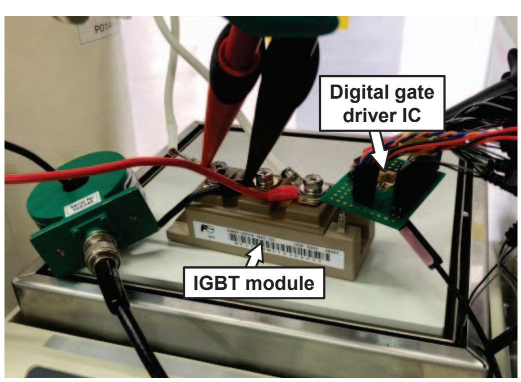

Fig. 4. Photo of measurement setup of double pulse test of IGBT module.

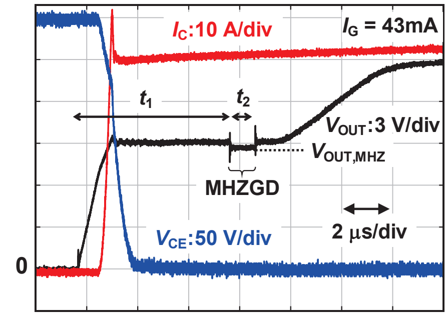

(a)

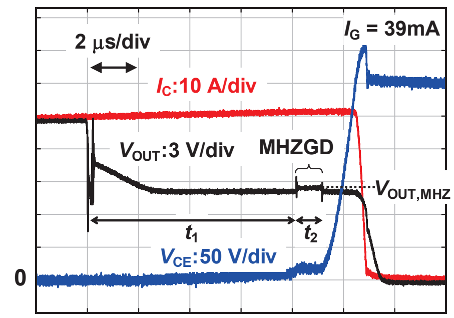

(b)

Fig. 5. Measured waveforms at I_L = 50 A, T_J = 25 °C, and t_2 = 1 µs. (a) Turn-on. (b) Turn-off.

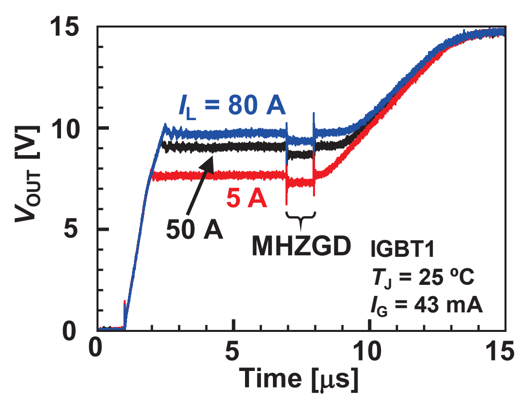

(a)

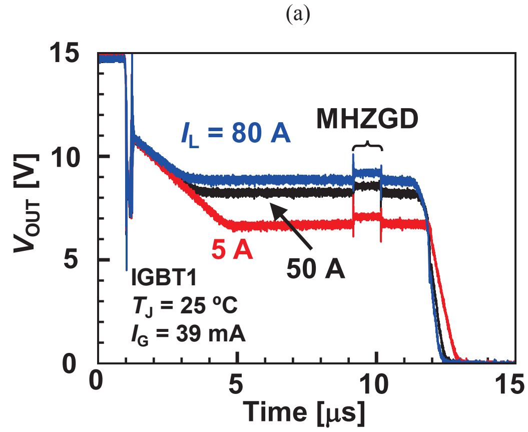

(b)

Fig. 6. Measured V_{OUT} waveforms of I_L = 5 A, 50 A and 80 A at T_J = 25 °C. (a) Turn-on. (b) Turn-off.

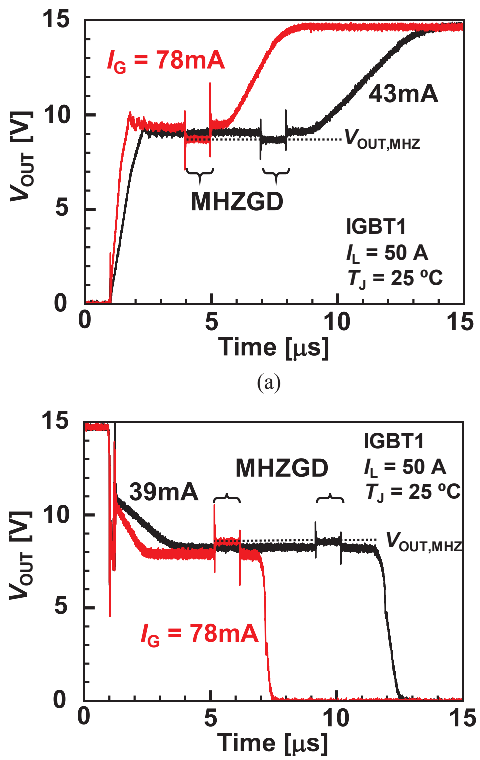

Fig. 7. Measured V_{OUT} waveforms of two different I_G's at I_L = 50 A and T_J = 25 °C. (a) Turn-on. (b) Turn-off.

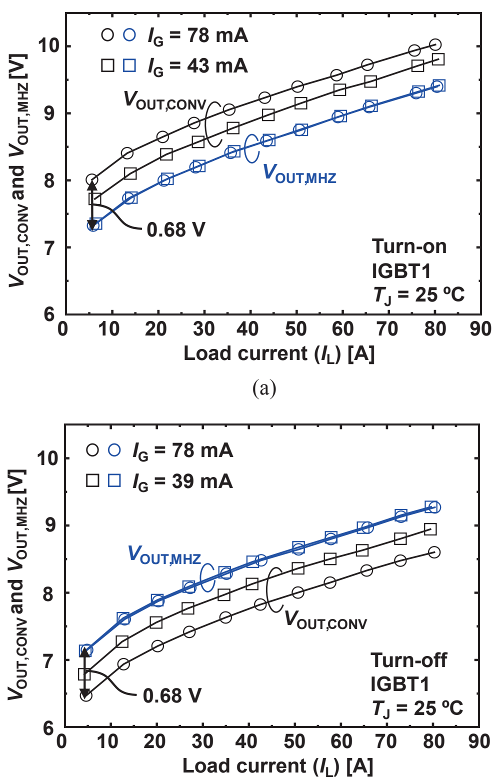

Fig. 8. Measured I_L dependence of $V_{OUT,CONV}$ and $V_{OUT,MHZ}$ of two different I_G's at T_J = 25 °C. (a) Turn-on. (b) Turn-off.

both turn-on and turn-off. Therefore, only the turn-on case will be discussed in the following sections.

III. Load Current Estimation Using MHZGD

In this section, the proposed I_L estimation method using MHZGD is explained. Eq. (1) shows the I_C model [10] based on alpha-power law model of MOSFET [11], where $k(T_J)$ is the T_J-dependent constant, $V_{TH}(T_J)$ is the T_J-dependent threshold voltage of IGBT, and α ($1 < \alpha < 2$) is a constant. Substituting $I_C = I_L$ and $V_{GE,INT} = V_{OUT,MHZ}$ into Eq. (1), Eq. (2) is obtained. Eq. (3) shows T_J dependence of $k(T_J)$ [12], where T_R is the room temperature (25 °C) whose unit is absolute temperature, $k(T_R)$ is $k(T_J)$ at $T_J = T_R$, and β ($\beta > 0$) is a constant. Eq. (3) shows T_J dependence of $V_{TH}(T_J)$ [12], where $V_{TH}(T_R)$ is $V_{TH}(T_J)$ at $T_J = T_R$, and γ ($\gamma > 0$) is a constant. Substituting Eqs. (3) and (4) into Eq. (2), Eq. (5) is obtained.

$$I_C = k(T_J)\left\{V_{GE,INT} - V_{TH}(T_J)\right\}^{\alpha} \quad (1)$$

$$I_L = k(T_J)\left\{V_{OUT,MHZ} - V_{TH}(T_J)\right\}^{\alpha} \quad (2)$$

$$k(T_J) = k(T_R)\left(\frac{T_J}{T_R}\right)^{-\beta} \quad (3)$$

$$V_{TH}(T_J) = V_{TH}(T_R) - \gamma\left(T_J - T_R\right) \quad (4)$$

$$I_L = k(T_R)\left(\frac{T_J}{T_R}\right)^{-\beta}\left\{V_{OUT,MHZ} - \left\{V_{TH}(T_R) - \gamma\left(T_J - T_R\right)\right\}\right\}^{\alpha} \quad (5)$$

Fig. 9 shows an overview of the proposed I_L estimation method using MHZGD. When the measured $V_{OUT,MHZ}$ and T_J are given, I_L is estimated using Eq. (5). $k(T_R)$, $V_{TH}(T_R)$, α, β, and γ are determined by the calibration method. Fig. 10 shows the calibration method for finding the values of five parameters. For unknown IGBTs, five parameters are determined by performing a five-point calibration from step 1 to step 5 only for the first one IGBT, and one parameter ($V_{TH}(T_R)$) is determined by performing a one-point calibration from step 6 to step 7 for the second and subsequent IGBTs. In Step 1, three $V_{OUT,MHZ}$'s are measured at three different I_L's at $T_J = T_R = 25$ °C. In Step 2, $k(T_R)$, $V_{TH}(T_R)$, and α are determined by the curve fitting [13] as shown in Fig. 11 (a). In Step 3, two $V_{OUT,MHZ}$'s are measured at two different I_L's at $T_J = 125$ °C. In Step 4, $k(T_J = 125$ °C) and $V_{TH}(T_J = 125$ °C)

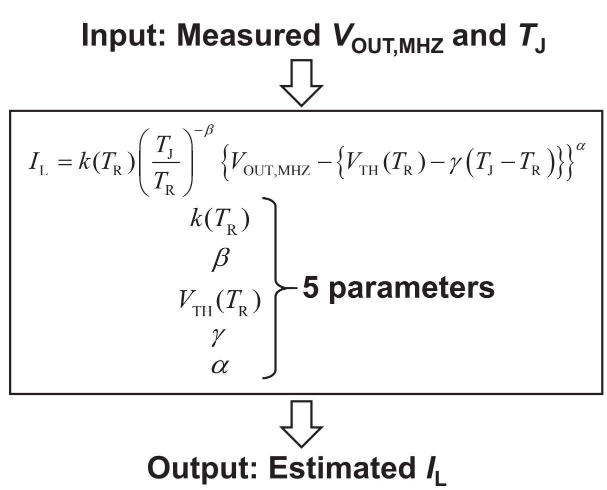

Fig. 9. Overview of proposed I_L estimation method using MHZGD.

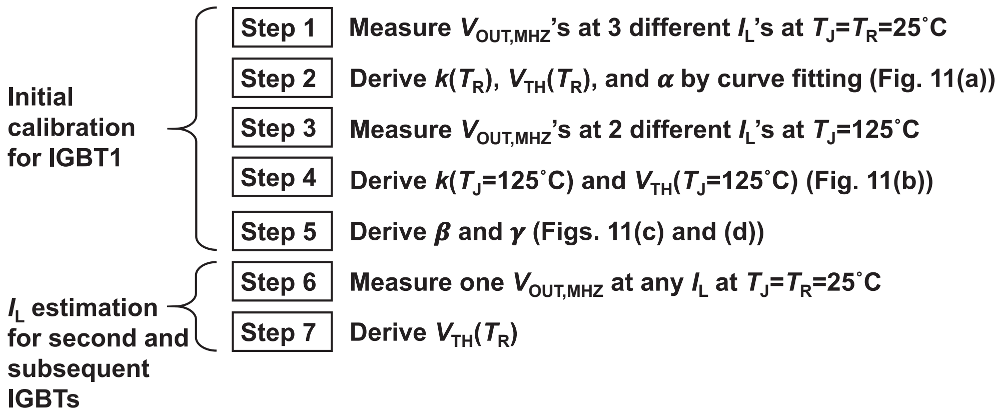

Fig. 10. Calibration method for finding values of five parameters.

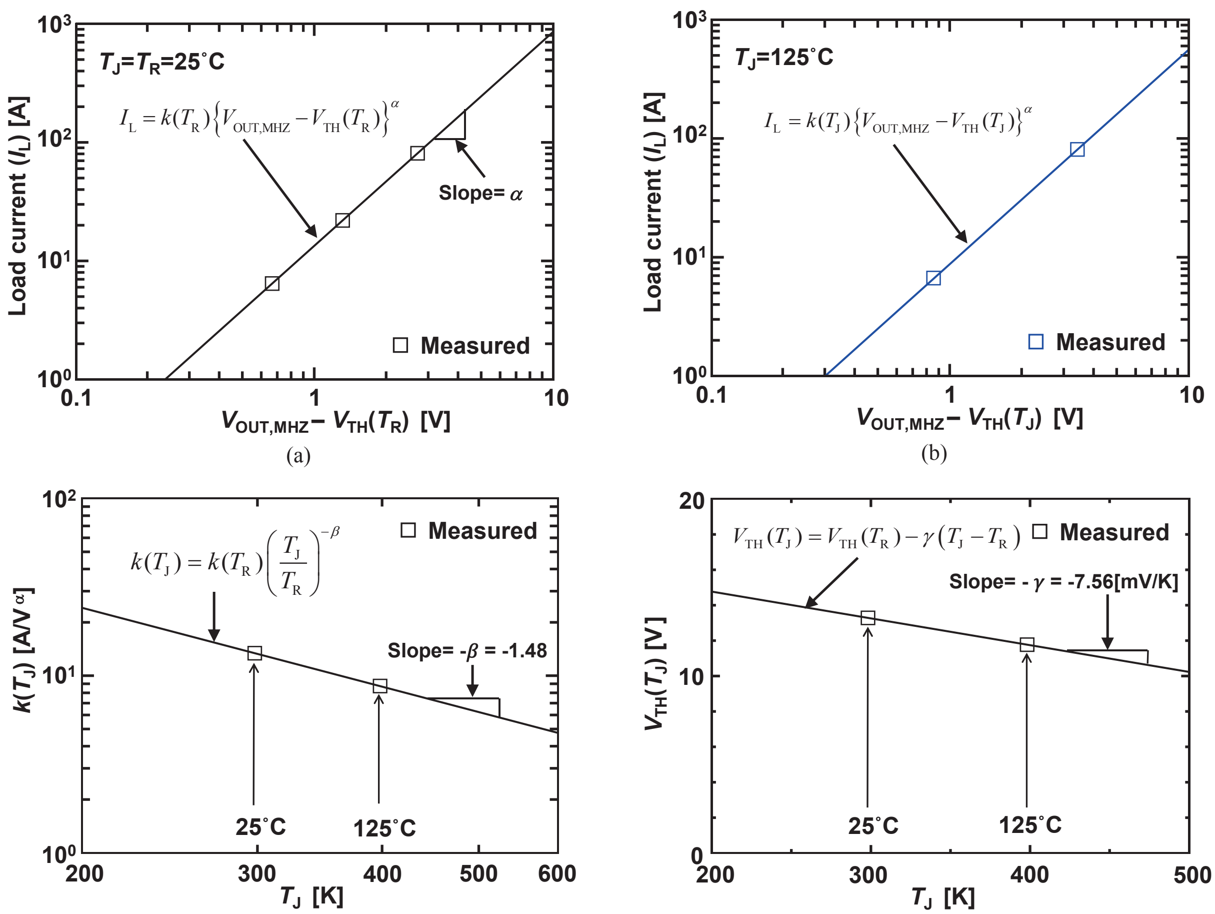

Fig. 11. Example of determination of parameters. (a) Step 2 in Fig. 10. (b) Step 4. (c) and (d) Step 5.

are determined by the curve fitting as shown in Fig. 11 (b). In Step 5, β and γ are determined by the curve fitting as shown in Figs. 11 (c) and (d). This completes the five-point calibration only for the first one IGBT. For the second and subsequent IGBTs, the same $k(T_R)$, α, β, and γ as the first one IGBT are used, and the one-point calibration from step 6 to step 7 are required to determine $V_{TH}(T_R)$ for each IGBT to account for manufacturing variations between IGBTs. In Step 6, one $V_{OUT,MHZ}$ is measured at any I_L at T_J = T_R = 25 °C. In Step 7, $V_{TH}(T_R)$ is determined by the curve fitting. Different from the model-based prediction which requires eight I_L measurements [8], the proposed estimation requires only one I_L measurement.

Table I shows the measurement conditions and the calibrated parameters obtained by the calibration method shown in Fig. 10. IGBT1 indicates the first one IGBT, and IGBT2,3 show the second and third IGBTs. In IGBT1, the five parameters are calibrated, while the one parameter ($V_{TH}(T_R)$) is calibrated in IGBT2 and IGBT3. Fig. 12 shows the measured and estimated I_L dependence of $V_{OUT,MHZ}$ of IGBT1 at T_J = 25 °C to 125 °C in 10 °C increments. The estimated

TABLE I. Measurement Conditions and Calibrated Parameters in One-Point Calibration

Measured conditions (T_J, I_L)	Sample	Calibrated parameters	Parameters				
			$V_{TH}(T_R)$ [V]	$k(T_R)$ [A/V$^{\alpha}$]	α	β	γ [mV/K]
(25˚C, 5A), (25˚C, 20A), (25˚C, 80A), (125˚C, 5A), (125˚C, 80A)	IGBT1	$V_{TH}(T_R)$, $k(T_R)$, α, γ, β	6.64	13.4	1.80	1.48	7.56
(25˚C, 5A)	IGBT2	$V_{TH}(T_R)$	6.83				
	IGBT3	$V_{TH}(T_R)$	6.87				

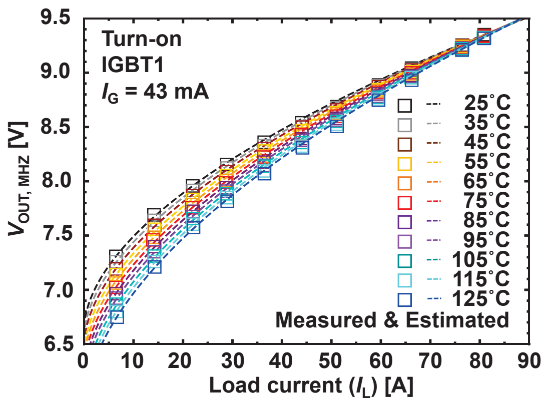

Fig. 12. Measured and estimated I_L dependence of $V_{OUT,MHZ}$ of IGBT1 at T_J = 25 °C to 125 °C in 10 °C increments.

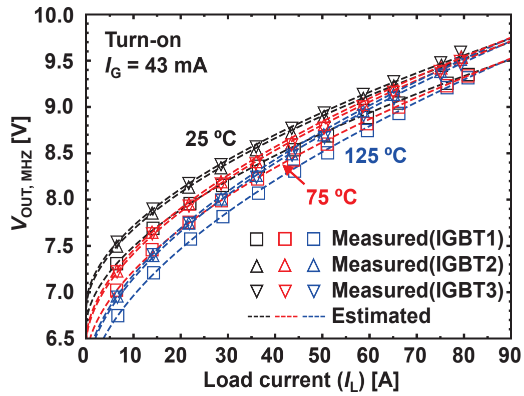

Fig. 14. Measured and estimated I_L dependence of $V_{OUT,MHZ}$ of IGBT1-3 at T_J = 25 °C, 75 °C, and 125 °C.

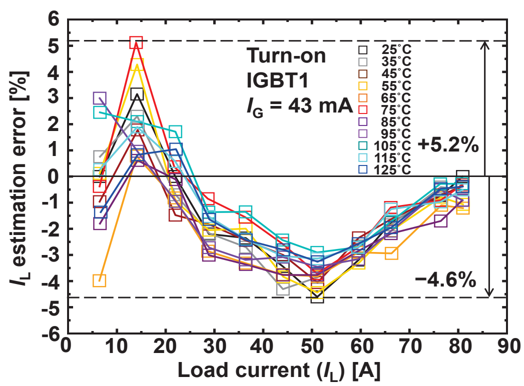

Fig. 13. I_L estimation error in Fig. 12.

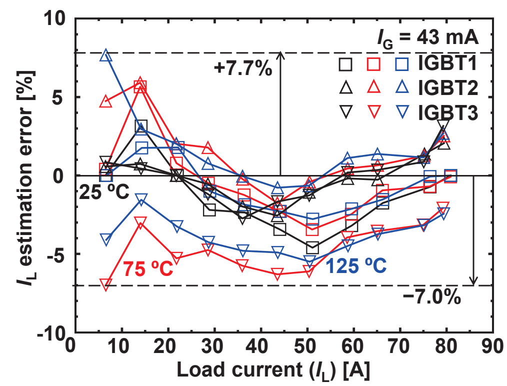

Fig. 15. I_L estimation error in Fig. 14.

curves are calculated using Eq. (5) and Table I. Fig. 13 shows the I_L estimation error in Fig. 12. I_L estimation error in IGBT1 in the range of 5 A to 80 A and T_J = 25 °C to 125 °C is within + 5.2 % / − 4.6 %, which supports that T_J dependence of I_L is reasonably expressed in Eq. (5) with β and γ. Fig. 14 shows the measured and estimated I_L dependence of $V_{OUT,MHZ}$ of IGBT1 to IGBT3 at T_J = 25 °C, 75 °C, and 125 °C. Fig. 15 shows the I_L estimation error in Fig. 14. Please note that I_L estimation errors at I_L = 20 A in IGBT2 and IGBT3 are 0 %, because the one-point calibration is done at I_L = 20 A. I_L estimation error of three IGBTs in the range of 5 A to 80 A at T_J = 25 °C, 75 °C, and 125 °C is within + 7.7 % / − 7.0 %, which supports that the manufacturing variations between IGBTs are reasonably expressed in Eq. (5) with different $V_{TH}(T_R)$ for each IGBT shown in Table I.

IV. Discussion on Number of Calibration Points

In the previous section, the one-point calibration is applied to IGBT2 and IGBT3, and I_L estimation error is within + 7.7 % / − 7.0 % as shown in Fig. 15. Increasing the number of points in the calibration can be considered as a way to reduce the I_L estimation error. When the number of calibration points is increased, however, the cost of the calibration for each IGBT will increase. To find out if increasing the number of points in the calibration would decrease the I_L estimation error, the relationship between the number of points in the calibration and the I_L estimation error is investigated in this section. Table II shows the measurement conditions and calibrated parameters obtained by five-point, four-point, and two-point calibrations. In the five-point calibration, the five parameters ($k(T_R)$, $V_{TH}(T_R)$, α, β, and γ) for each IGBT are determined by

TABLE II. MEASUREMENT CONDITIONS AND CALIBRATED PARAMETERS.

Measured conditions (T_J, I_L)	Sample	Calibrated parameters	Parameters				
			$V_{TH}(T_R)$ [V]	$k(T_R)$ [A/V$^{\alpha}$]	α	β	γ [mV/K]
(25˚C, 5A), (25˚C, 20A), (25˚C, 80A), (125˚C, 5A), (125˚C, 80A)	IGBT1	$V_{TH}(T_R)$, $k(T_R)$, α, γ, β	6.64	13.4	1.80	1.48	7.56
	IGBT2	$V_{TH}(T_R)$, $k(T_R)$, α, γ, β	6.86	14.3	1.74	1.37	7.07
	IGBT3	$V_{TH}(T_R)$, $k(T_R)$, α, γ, β	6.92	14.7	1.71	1.21	7.41

(a) Five-point calibration.

Measured conditions (T_J, I_L)	Sample	Calibrated parameters	Parameters				
			$V_{TH}(T_R)$ [V]	$k(T_R)$ [A/V$^{\alpha}$]	α	β	γ [mV/K]
(25˚C, 5A), (25˚C, 20A), (25˚C, 80A), (125˚C, 5A), (125˚C, 80A)	IGBT1	$V_{TH}(T_R)$, $k(T_R)$, α, γ, β	6.64	13.4	1.80	1.48	7.56
(25˚C, 5A), (25˚C, 80A), (125˚C, 5A), (125˚C, 80A)	IGBT2	$V_{TH}(T_R)$, $k(T_R)$, γ, β	6.82	13.1		1.42	7.18
	IGBT3	$V_{TH}(T_R)$, $k(T_R)$, γ, β	6.85	12.9		1.28	7.56

(b) Four-point calibration.

Measured conditions (T_J, I_L)	Sample	Calibrated parameters	Parameters				
			$V_{TH}(T_R)$ [V]	$k(T_R)$ [A/V$^{\alpha}$]	α	β	γ [mV/K]
(25˚C, 5A), (25˚C, 20A), (25˚C, 80A), (125˚C, 5A), (125˚C, 80A)	IGBT1	$V_{TH}(T_R)$, $k(T_R)$, α, γ, β	6.64	13.4	1.80	1.48	7.56
(25˚C, 5A), (25˚C, 80A)	IGBT2	$V_{TH}(T_R)$, $k(T_R)$	6.82	13.1			
	IGBT3	$V_{TH}(T_R)$, $k(T_R)$	6.85	12.9			

(c) Two-point calibration.

the calibration method shown in Fig. 10. In the four-point calibration, the five parameters are calibrated in IGBT1, while the four parameter ($k(T_R)$, $V_{TH}(T_R)$, β, and γ) is calibrated in IGBT2 and IGBT3. In the two-point calibration, the five parameters are calibrated in IGBT1, while the two parameter ($k(T_R)$ and $V_{TH}(T_R)$) is calibrated in IGBT2 and IGBT3.

Fig. 16 shows the I_L estimation error of three IGBTs at T_J = 25 °C, 75 °C, and 125 °C in five-point, four-point, and two-point calibrations. Table III shows a summary of the I_L estimation error in four different calibration methods. When the number of calibration points is increased from one to five, the range of the I_L estimation error decreases from 14.7 % to 11.1 %. The five-point calibration, however, requires five measurements at T_J = 25 °C and 125 °C for each IGBT, which is not practical, because the calibration cost is high. Therefore, in conclusion, the one-point calibration is recommended and proposed in this paper. In Table III, it is not reasonable at first glance for the error range of two-point calibration to be larger than that of one-point calibration. The reason is that the two-point calibration is done at I_L = 5 A and 80 A as shown in Fig. 16 (c) and the one-point calibration is done at I_L = 20 A as shown in Fig. 15, and the I_L estimation error range of the one-point calibration is accidentally small in this case.

V. CONCLUSIONS

The proposed MHZGD, which can be integrated on DGD IC, estimated I_L from $V_{OUT,MHZ}$ without depending on I_G, and I_L estimation errors of three IGBTs were within + 7.7 % / − 7.0 % using the one-point calibration in the range of 5 A to 80 A at 25 °C, 75 °C, and 125 °C. When the number of calibration points is increased from one to five, the I_L estimation error range decreases from 14.7 % to 11.1 %. The one-point calibration, however, is recommended, because the cost of the five-point calibration at T_J = 25 °C and 125 °C for each IGBT is excessive.

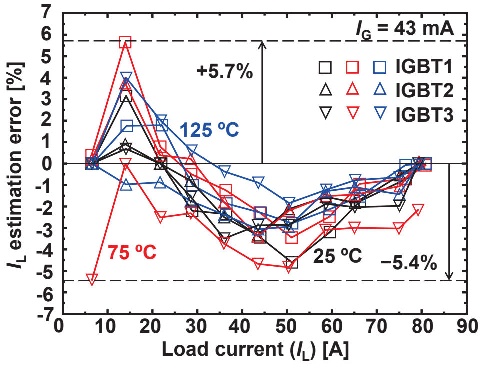

(a)

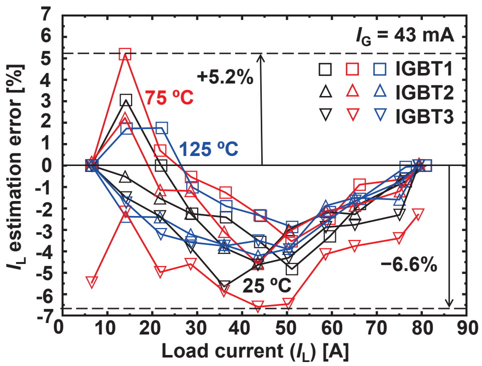

(b)

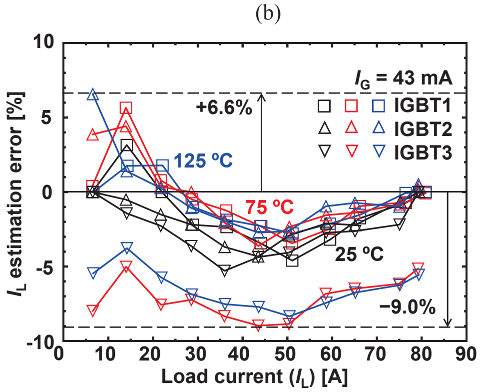

(c)

Fig. 16. I_L estimation error of IGBT1-3 at T_J = 25 °C, 75 °C, and 125 °C in (a) five-point, (b) four-point, and (c) two-point calibrations.

TABLE III. SUMMARY OF I_L ESTIMATION ERROR IN FOUR DIFFERENT CALIBRATION METHODS

Calibration method	I_L estimation error		
	Max	Min	Max − Min
5-point	+5.7%	−5.4%	11.1%
4-point	+5.2%	−6.6%	11.8%
2-point	+6.6%	−9.0%	15.6%
1-point	+7.7%	−7.0%	14.7%

ACKNOWLEGEMENT

This work was partly supported by JST-Mirai Program, Grant Number JPMJMI20E1, Japan.

REFERENCES

[1] K. Miyazaki, S. Abe, M. Tsukuda, I. Omura, K. Wada, M. Takamiya, and T. Sakurai, "General-purpose clocked gate driver IC with programmable 63-level drivability to optimize overshoot and energy loss in switching by a simulated annealing algorithm," *IEEE Trans. on Industry Applications*, vol. 53, issue 3, pp. 2350–2357, May-Jun. 2017.

[2] T. Sai, K. Miyazaki, H. Obara, T. Mannen, K. Wada, I. Omura, M. Takamiya, and T. Sakurai, "Load current and temperature dependent optimization of active gate driving vectors," in *Proc. IEEE Energy Conversion Congress and Exposition*, Sep. 2019, pp. 3292–3297.

[3] D. Gu and P. Kshirsagar, "Compact integrated gate drives and current sensing solution for SiC power modules," in *Proc. IEEE Energy Conversion Congress and Exposition*, Oct. 2017, pp. 5139-5143.

[4] E. Preuss, E. -P. Eni, and W. Frank, "Optimize the integrated overcurrent protection of gate driver ICs for current sense range extension," in *Proc. PCIM Asia 2020; International Exhibition and Conference for Power Electronics, Intelligent Motion, Renewable Energy and Energy Management*, Nov. 2020, pp. 1-5.

[5] J. Wang, Z. Shen, C. DiMarino, R. Burgos, and D. Boroyevich, "Gate driver design for 1.7kV SiC MOSFET module with Rogowski current sensor for shortcircuit protection," in *Proc. IEEE Applied Power Electronics Conference and Exposition*, Mar. 2016, pp. 516-523.

[6] J. Wang, S. Mocevic, Y. Xu, C. DiMarino, R. Burgos, and D. Boroyevich, "A high-speed gate driver with PCB-embedded Rogowski switch-current sensor for a 10 kV, 240 A, SiC MOSFET module," in *Proc. IEEE Energy Conversion Congress and Exposition*, Sep. 2018, pp. 5489-5494.

[7] Q. Nie, H. Peng, and Y. Kang, "An ultra-fast gate driver with over current protection for GaN power transistors," *in Proc. 22nd European Conference on Power Electronics and Applications*, 2020, pp. 1-7.

[8] C. H. van der Broeck, A. Gospodinov, and R. W. De Doncker, "IGBT junction temperature estimation via gate voltage plateau sensing," *IEEE Trans. on Industry Applications*, vol. 54, issue 5, pp. 4752-4763, Sep.-Oct. 2018.

[9] J. Chen, W. J. Zhang, A. Shorten, J. Yu, M. Sasaki, T. Kawashima, H. Nishio, and W. T. Ng, "a smart IGBT gate driver IC with temperature compensated collector current sensing," *IEEE Trans. on Power Electronics*, vol. 34, issue 5, pp. 4613-4627, May 2019.

[10] K. Miyazaki, K. Wada, I. Omura, M. Takamiya, and T. Sakurai, "Gate waveform optimization in emergency turn-off of IGBT using digital gate driver," *10th International Conference on Power Electronics and ECCE Asia*, May 2019, pp. 3292-3296.

[11] T. Sakurai and A. R. Newton, "Alpha-power law MOSFET model and its applications to CMOS inverter delay and other formulas," *IEEE Journal of Solid-State Circuits*, vol. 25, issue 2, pp. 584-594, Apr. 1990.

[12] N. H. E. Weste and D. M. Harris, "CMOS VLSI design: a circuits and systems perspective", Fourth edition, Boston, MA, USA, Addison-Wesley, 2010.

[13] D. Marquardt, "An algorithm for least-squares estimation of nonlinear parameters", *Journal of the Society for Industrial and Applied Mathematics*, vol. 11, No. 2, pp. 431–441, June 1963.